PERGAMON

International Journal of Heat and Mass Transfer 43 (2000) 2009–2020

International Journal of HEAT and MASS TRANSFER

www.elsevier.com/locate/ijhmt

Integral equation formulation for transient radiative transfer in an anisotropically scattering medium

Chih-Yang Wu*, Shang-Hsuang Wu

Department of Mechanical Engineering, National Cheng Kung University, Tainan, Taiwan 701, Republic of China

Received 19 February 1999; received in revised form 16 June 1999

Abstract

The integral equation formulation for transient radiative transfer in a 3D absorbing and anisotropically scattering medium is developed. The method developed is applied to transient radiative transfer in 1D planar and 2D cylindrical linearly anisotropically scattering media exposed to pulse radiation. The integral equations for the two examples are solved by the quadrature method. The results by the present method agree quite well with those obtained by the Monte Carlo methods. The effects of various parameters are investigated. © 2000 Elsevier Science Ltd. All rights reserved.

Keywords: Transient radiative transfer; Anisotropic scattering; Integral equation; Pulse irradiation

1. Introduction

More and more studies on transient radiative transfer in a participating medium exposed to a laser pulse have appeared recently with the impetuses from a variety of engineering and clinical applications, such as atmosphere remote sensing [1,2], oceanographic lidar [3], thermal (or optical) tomography [4], photodynamic therapy [5], and estimating radiative properties of participating media [6,7]. Since transient radiative transfer is governed by an integro-differential equation, which is complex to solve analytically even in a 1D planar medium, the studies adopt approximate methods or Monte Carlo methods to solve the equation of transient radiative transfer. The Monte Carlo method [8], in essence, is a stochastic (or statistical) method. It is flexible to handle complex geometrical shapes, anisotropic scattering and nonhomogeneous properties, but the results obtained by the method always have unavoidable random errors due to practical finite samplings. In contrast, deterministic methods do not suffer the defect, and so they are sometimes preferred. Among the popular deterministic methods, the adding/doubling method is proposed to solve the transient response of a medium with a unit-step external source [9]. The parabolic diffuse approximation is applied to evaluating the reflected and the transmitted intensities of a scattering slab with pulse irradiation [6,10]. Mitra and Kumar [11] consider light-pulse transport through scattering–absorbing media, and directly compare the performances of various approximate methods, including the hyperbolic $P-1$ and some low order P–N approximations, the two-flux model, and the discrete-ordinate method. However, these studies are merely focused on the geometrically simplest case, a 1D planar medium. On the other hand, only very few studies are devoted to multi-dimensional transient

* Corresponding author. Fax: +886-6-235-2973.

0017-9310/00/$ - see front matter
PII: S0017-9310(99)00262-8

Nomenclature

a_n	phase function coefficients
a_{nm}	coefficients in the expression of phase function in terms of spherical harmonics, see Eq. (8)
c	speed of light in the medium
$\mathbf{e}_1$, $\mathbf{e}_2$, $\mathbf{e}_3$	unit vectors in the u_1-, u_2- and u_3-directions, respectively
$\mathbf{e}_r$, $\mathbf{e}_\psi$, $\mathbf{k}$	unit vectors in the r-, ψ- and z-directions, respectively
F	function describing the temporal shape of the pulse, see Eq. (16)
I	radiation intensity
I_o	peak value of the pulse
M_{nm}, M^*_{nm}	moments of intensity, defined in Eq. (11)
$\mathbf{n}$	unit normal vector
N	order of the anisotropic scattering
N_φ, N_μ, N_s	quadrature point numbers for the φ, μ and s integrations, respectively
$\mathbf{q}$	radiative flux
r, ψ, z	cylindrical coordinates, see Fig. 1(b)
$\mathbf{r}$	position vector
r_o, z_o	radius and height of the cylindrical medium, respectively
Δr, Δz, Δt	grid sizes in the r-, z- and t-directions, respectively
s	distance measured from position $\mathbf{r}$ along the direction $-\boldsymbol{\Omega}$
S	source function
t	time
t_c	time when the peak of the pulse entering the medium
t_p	full width at half maximum for the temporal shape of $F(t)$
u_1, u_2, u_3	orthogonal curvilinear coordinates

Greek symbols

β	extinction coefficient
δ_{0m}	function defined in Eq. (9)
ζ	function defined in Eq. (25)
θ	polar angle
Λ	function describing the initial distribution of I
μ	cosine of θ
τ	optical distance
φ	azimuthal angle
Φ	phase function
ω	scattering albedo
Ω	solid angle
$\boldsymbol{\Omega}$	unit vector in a direction

Subscripts

u	upper limit
w	boundary

Superscript

−	leaving the medium

radiative transfer. Very recently, Yamada and Hasegawa [12] employ the finite element method to solve the parabolic diffuse approximation equation to analyze the transient radiative transfer in 2D and 3D cylindrical media with light impulses, while Mitra and coworkers [13] apply the hyperbolic $P-1$ approximation to the transient radiative transfer within a 2D rectangular medium. To assess the accuracy of the solutions obtained by the approximate methods, highly accurate solutions based on exact formulation are required.

Highly accurate solutions of the integral equation for time-independent radiative transfer have been obtained [14,15]. Moreover, Wu [16] has developed the integral equation of transient radiative transfer in an isotropically scattering planar medium, and it is shown that the integral equation can be solved accurately by a quadrature method (QM). Hence, the integral equation approach seems to be promising.

In this work, we first develop the integral equation formulation for transient radiative transfer in a general 3D anisotropically scattering medium. The formulation for transient radiative transfer, to the best of our knowledge, has not been derived yet. Then, the formulation is applied to studying transient radiative transfer in 1D planar and 2D cylindrical linearly anisotropically scattering media with pulse irradiation. The QM, an adaptation of the method proposed in [16], is used to solve the resulting integral equations. To validate the solutions, the integral equation results obtained by the QM are compared with the results solved by the Monte Carlo methods.

2. General formulation

In an absorbing and scattering medium with constant radiative properties, the radiative intensity I at position $\mathbf{r}$ along direction $\boldsymbol{\Omega}$ at time t can be described by the equation of transient radiative transfer

$$\frac{1}{c}\frac{\partial I(\mathbf{r}, \boldsymbol{\Omega}, t)}{\partial t} + \boldsymbol{\Omega}\cdot\nabla I(\mathbf{r}, \boldsymbol{\Omega}, t) + \beta I(\mathbf{r}, \boldsymbol{\Omega}, t) = \beta S(\mathbf{r}, \boldsymbol{\Omega}, t) \tag{1}$$

where c is the speed of light in the medium, β the extinction coefficient, and S the source function defined as

$$S(\mathbf{r}, \boldsymbol{\Omega}, t) = \frac{\omega}{4\pi}\int_{4\pi} I(\mathbf{r}, \boldsymbol{\Omega}', t)\Phi(\boldsymbol{\Omega}'\cdot\boldsymbol{\Omega})\,\mathrm{d}\boldsymbol{\Omega}', \tag{2}$$

Here, ω is the scattering albedo, Φ the phase function, and $\mathrm{d}\Omega'$ an infinitesimal solid angle around the incoming direction $\boldsymbol{\Omega}'$. Here, a cold medium is considered; that is, the emission of the medium is negligibly small as compared to the irradiation at the medium boundary. The scattering is instantaneous or of no retention time [17]. The notation denoting the spectral dependence of the radiative properties has been omitted to simplify the mathematical formulations, and so Eq. (1) is valid for monochromatic or gray radiative transfer. Moreover, the geometrical sizes of the considered medium are assumed to be much larger than wavelength, the boundary of the medium is non-participating, and the medium of interest is non-re-entrant. By non-re-entrant we mean that any radiative energy leaving the medium surface will not re-enter the medium through another part of the surface [18].

The required initial and boundary conditions of Eq. (1) can be expressed as

$$I(\mathbf{r}, \boldsymbol{\Omega}, 0) = \Lambda(\mathbf{r}, \boldsymbol{\Omega}) \tag{3}$$

$$I(\mathbf{r}_\mathrm{w}, \boldsymbol{\Omega}, t) = I_\mathrm{w}(\mathbf{r}_\mathrm{w}, \boldsymbol{\Omega}, t), \quad \boldsymbol{\Omega}\cdot\mathbf{n} > 0,\ t \geq 0 \tag{4}$$

where Λ and I_w are two specified functions with $\mathbf{r}$ and $\mathbf{r}_\mathrm{w}$ denoting locations in the medium and on the boundary surface, respectively, and $\mathbf{n}$ is the unit normal vector at $\mathbf{r}_\mathrm{w}$ pointing to the medium.

The incident radiation (or the integrated intensity) can be defined as

$$M_{00}(\mathbf{r}, t) = \int_{4\pi} I(\mathbf{r}, \boldsymbol{\Omega}, t)\,\mathrm{d}\Omega \tag{5}$$

M_{00} is a quantity independent of direction and is of particular interest. An integral expression of M_{00}, in terms of the source function can be derived [18]. The expression is an integral equation of M_{00} if the scattering is isotropic, and so the expression is useful. However, in the general case of anisotropic scattering, the expression represents an identity rather than an equation which can be solved for M_{00} [18]. It is found that the integral expression just mentioned, can be recast as a set of integral equations which can be solved for M_{00} and other moments of intensity by expanding the phase function in a series of Legendre

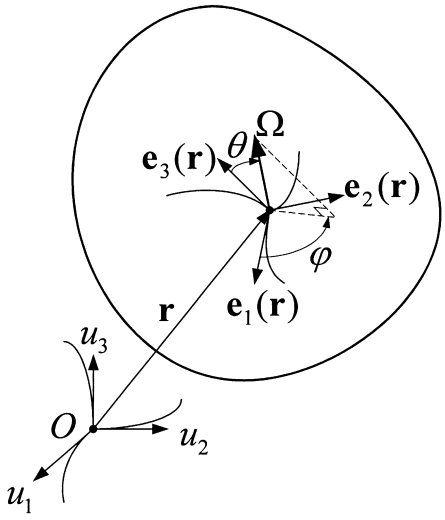

(a)

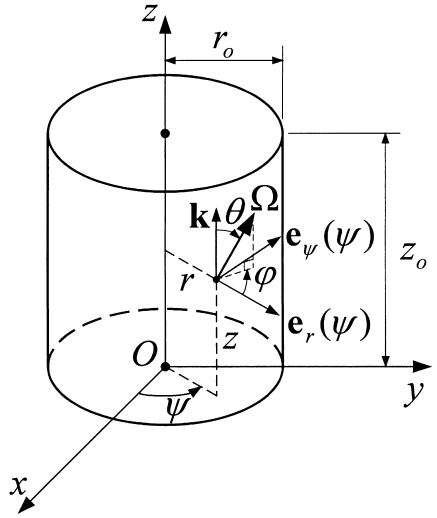

(b)

Fig. 1. The geometries of the media considered and the coordinate systems; (a) an arbitrary 3D medium; (b) a finite cylindrical medium.

polynomials. The series expansion of the phase function in terms of the Legendre polynomials was proposed by Chu and Churchill [19].

Before deriving the set of integral equations for radiative transfer in an anisotropically scattering medium, the spatial and the directional coordinate systems are specified. Here, we adopt an orthogonal curvilinear coordinate system with coordinates labeled with u_1, u_2 and u_3 to describe spatial positions, and the directional polar axis is aligned with the spatial u_3 direction, while the directional azimuthal angle is the angle between the tangent of the u_1 curve and the projection of $\boldsymbol{\Omega}$ in the u_1u_2 plane. The spatial and the directional coordinate systems are shown in Fig. 1(a). Then, at position $\mathbf{r}$, an arbitrary direction $\boldsymbol{\Omega}$ can be expressed as

$$\begin{aligned}\boldsymbol{\Omega} = {} & \left\{1-\left[\mu(\boldsymbol{\Omega};\mathbf{r})\right]^2\right\}^{1/2}\cos\left[\varphi(\boldsymbol{\Omega};\mathbf{r})\right]\mathbf{e}_1(\mathbf{r}) + \left\{1\right. \\ & \left. -\left[\mu(\boldsymbol{\Omega};\mathbf{r})\right]^2\right\}^{1/2}\sin\left[\varphi(\boldsymbol{\Omega};\mathbf{r})\right]\mathbf{e}_2(\mathbf{r}) \\ & +\mu(\boldsymbol{\Omega};\mathbf{r})\mathbf{e}_3(\mathbf{r}) \end{aligned} \tag{6}$$

where $\mathbf{e}_1(\mathbf{r})$, $\mathbf{e}_2(\mathbf{r})$ and $\mathbf{e}_3(\mathbf{r})$ are unit vectors in the u_1-, u_2- and u_3-directions, respectively, $\mu(\boldsymbol{\Omega};\mathbf{r})=\cos[\theta(\boldsymbol{\Omega};\mathbf{r})]$, and $\theta(\boldsymbol{\Omega};\mathbf{r})$ and $\varphi(\boldsymbol{\Omega};\mathbf{r})$, are the polar angle and the azimuthal angle for $\boldsymbol{\Omega}$ at position $\mathbf{r}$, respectively. The explicit expressions of $\theta(\boldsymbol{\Omega};\mathbf{r})$ and $\varphi(\boldsymbol{\Omega};\mathbf{r})$ are dependent on the coordinate systems used, and can be determined by

$$\left\{1-\left[\mu(\boldsymbol{\Omega};\mathbf{r})\right]^2\right\}^{1/2}\cos\left[\varphi(\boldsymbol{\Omega};\mathbf{r})\right] = \boldsymbol{\Omega}\cdot\mathbf{e}_1(\mathbf{r}) \tag{7a}$$

$$\left\{1-\left[\mu(\boldsymbol{\Omega};\mathbf{r})\right]^2\right\}^{1/2}\sin\left[\varphi(\boldsymbol{\Omega};\mathbf{r})\right] = \boldsymbol{\Omega}\cdot\mathbf{e}_2(\mathbf{r}) \tag{7b}$$

$$\mu(\boldsymbol{\Omega};\mathbf{r}) = \boldsymbol{\Omega}\cdot\mathbf{e}_3(\mathbf{r}) \tag{7c}$$

With the addition theorem for the Legendre polynomials, the phase function can be expressed in terms of the spherical harmonics [20]

$$\begin{aligned}\Phi(\boldsymbol{\Omega}'\cdot\boldsymbol{\Omega}) = {} & \sum_{m=0}^{N}\sum_{n=m}^{N}(2-\delta_{0m})a_{nm}P_n^m\left[\mu(\boldsymbol{\Omega};\mathbf{r})\right] \\ & \times P_n^m\left[\mu(\boldsymbol{\Omega}';\mathbf{r})\right]\cos\left\{m\left[\varphi(\boldsymbol{\Omega};\mathbf{r})-\varphi(\boldsymbol{\Omega}';\mathbf{r})\right]\right\}\end{aligned} \tag{8}$$

where $a_{nm}=a_n(n-m)!/(n+m)!$, $a_0=1$, and δ_{0m} is defined as

$$\delta_{0m}=\begin{cases}1 & \text{for } m=0\\ 0 & \text{for } m\neq 0\end{cases} \tag{9}$$

The terms after the Nth one are truncated for the Nth-degree anisotropic scattering approximation. It is worthy of mentioning that the expression of phase function, Eq. (8), is in terms of the directional coordinate system adopted. If another directional coordinate system is used, the expression varies.

Substituting Eq. (8) into Eq. (2), we obtain

$$\begin{aligned}S(\mathbf{r},\boldsymbol{\Omega},t) = {} & \frac{\omega}{4\pi}\sum_{m=0}^{N}\sum_{n=m}^{N}(2-\delta_{0m})a_{nm}P_n^m\left[\mu(\boldsymbol{\Omega};\mathbf{r})\right] \\ & \times\left\{\cos\left[m\varphi(\boldsymbol{\Omega};\mathbf{r})\right]M_{nm}(\mathbf{r},t)\right. \\ & \left.+\sin\left[m\varphi(\boldsymbol{\Omega};\mathbf{r})\right]M_{nm}^*(\mathbf{r},t)\right\}\end{aligned} \tag{10}$$

where the moments of intensity are defined as

$$\begin{aligned}\begin{Bmatrix}M_{nm}(\mathbf{r},t)\\ M_{nm}^*(\mathbf{r},t)\end{Bmatrix} = {} & \int_{4\pi} I(\mathbf{r},\boldsymbol{\Omega},t)P_n^m\left[\mu(\boldsymbol{\Omega};\mathbf{r})\right] \\ & \times\begin{Bmatrix}\cos\left[m\varphi(\boldsymbol{\Omega};\mathbf{r})\right]\\ \sin\left[m\varphi(\Omega;\mathbf{r})\right]\end{Bmatrix}\mathrm{d}\Omega\end{aligned} \tag{11}$$

for $m\le n\le N$, $0\le m\le N$. Substituting Eq. (10) into the formal solution of the intensity obtained from the integration of Eq. (1) [18], we have the formal solution of I in terms of the moments of intensity

$$\begin{aligned}I(\mathbf{r},\boldsymbol{\Omega},t) = {} & \Lambda(\mathbf{r}-ct\boldsymbol{\Omega},\boldsymbol{\Omega})\exp\left[-\tau(\mathbf{r},\mathbf{r}-ct\boldsymbol{\Omega})\right] \\ & \times H\left(\left|\mathbf{r}-\mathbf{r}_{\mathrm{w}}(\mathbf{r},\boldsymbol{\Omega})\right|-ct\right) \\ & + I_{\mathrm{w}}\left[\mathbf{r}_{\mathrm{w}}(\mathbf{r},\boldsymbol{\Omega}),\boldsymbol{\Omega},t-\left|\mathbf{r}-\mathbf{r}_{\mathrm{w}}(\mathbf{r},\boldsymbol{\Omega})\right|/c\right] \\ & \times\exp\left\{-\tau\left[\mathbf{r},\mathbf{r}_{\mathrm{w}}(\mathbf{r},\boldsymbol{\Omega})\right]\right\}H\left(ct-\left|\mathbf{r}-\mathbf{r}_{\mathrm{w}}(\mathbf{r},\boldsymbol{\Omega})\right|\right) \\ & +\frac{1}{4\pi}\int_0^{|\mathbf{r}-\mathbf{r}_{\mathrm{w}}(\mathbf{r},\boldsymbol{\Omega})|}\beta\omega\exp\left[-\tau(\mathbf{r},\mathbf{r}-s\boldsymbol{\Omega})\right] \\ & \times H(ct-s)\sum_{m=0}^{N}\sum_{n=m}^{N}(2-\delta_{0m})a_{nm} \\ & \times P_n^m\left[\mu(\boldsymbol{\Omega};\mathbf{r}-s\boldsymbol{\Omega})\right]\left\{\cos\left[m\varphi(\boldsymbol{\Omega};\mathbf{r}-s\boldsymbol{\Omega})\right]\right. \\ & \times M_{nm}(\mathbf{r}-s\boldsymbol{\Omega},t-s/c)+\sin\left[m\varphi(\boldsymbol{\Omega};\mathbf{r}-s\boldsymbol{\Omega})\right] \\ & \left.\times M_{nm}^*(\mathbf{r}-s\boldsymbol{\Omega},t-s/c)\right\}\mathrm{d}s\end{aligned} \tag{12}$$

where H is the Heaviside step function, $\tau(\mathbf{r},\mathbf{r}')=\beta|\mathbf{r}-\mathbf{r}'|$ is the optical distance between two points $\mathbf{r}$ and $\mathbf{r}'$, s is the distance measured from position $\mathbf{r}$ along the direction $-\boldsymbol{\Omega}$, and $\mathbf{r}_{\mathrm{w}}$ represents the nearest point on the medium boundary surface seen from $\mathbf{r}$ in the direction $-\boldsymbol{\Omega}$. Thus, $\mathbf{r}_{\mathrm{w}}$ is determined by $\mathbf{r}$, $\boldsymbol{\Omega}$, and the geometry of the medium boundary surface.

Substituting Eq. (12) into Eq. (11), we obtain the

integral equations of the moments of intensity

$$\begin{Bmatrix} M_{nm}(\mathbf{r},t) \\ M^*_{nm}(\mathbf{r},t) \end{Bmatrix} = \int_{4\pi} \Lambda(\mathbf{r}-ct\boldsymbol{\Omega},\boldsymbol{\Omega})\exp\big[-\tau(\mathbf{r},\mathbf{r}-ct\boldsymbol{\Omega})\big] \times H\big(|\mathbf{r}-\mathbf{r}_w(\mathbf{r},\boldsymbol{\Omega})|-ct\big)P_n^m\big[\mu(\boldsymbol{\Omega};\mathbf{r})\big] \times \begin{Bmatrix} \cos\big[m\varphi(\boldsymbol{\Omega};\mathbf{r})\big] \\ \sin\big[m\varphi(\boldsymbol{\Omega};\mathbf{r})\big] \end{Bmatrix} \mathrm{d}\Omega + \int_{4\pi} I_w\big[\mathbf{r}_w(\mathbf{r},\boldsymbol{\Omega}),\boldsymbol{\Omega},t-|\mathbf{r}-\mathbf{r}_w(\mathbf{r},\boldsymbol{\Omega})|/c\big] \times \exp\big\{-\tau\big[\mathbf{r},\mathbf{r}_w(\mathbf{r},\boldsymbol{\Omega})\big]\big\} \times H\big(ct-|\mathbf{r}-\mathbf{r}_w(\mathbf{r},\boldsymbol{\Omega})|\big)P_n^m\big[\mu(\boldsymbol{\Omega};\mathbf{r})\big] \times \begin{Bmatrix} \cos\big[m\varphi(\boldsymbol{\Omega};\mathbf{r})\big] \\ \sin\big[m\varphi(\boldsymbol{\Omega};\mathbf{r})\big] \end{Bmatrix} \mathrm{d}\Omega + \frac{1}{4\pi}\int_{4\pi}\int_0^{|\mathbf{r}-\mathbf{r}_w(\mathbf{r},\boldsymbol{\Omega})|} \beta\omega \times \exp\big[-\tau(\mathbf{r},\mathbf{r}-s\boldsymbol{\Omega})\big] \times H(ct-s)P_n^m\big[\mu(\boldsymbol{\Omega};\mathbf{r})\big] \times \begin{Bmatrix} \cos\big[m\varphi(\boldsymbol{\Omega};\mathbf{r})\big] \\ \sin\big[m\varphi(\boldsymbol{\Omega};\mathbf{r})\big] \end{Bmatrix} \times \sum_{j=0}^{N}\sum_{k=j}^{N}(2-\delta_{0j})a_{kj}P_k^j\big[\mu(\boldsymbol{\Omega};\mathbf{r}-s\boldsymbol{\Omega})\big] \times \Big\{\cos\big[j\varphi(\boldsymbol{\Omega};\mathbf{r}-s\boldsymbol{\Omega})\big] \times M_{kj}(\mathbf{r}-s\boldsymbol{\Omega},t-s/c) + \sin\big[j\varphi(\boldsymbol{\Omega};\mathbf{r}-s\boldsymbol{\Omega})\big] \times M^*_{kj}(\mathbf{r}-s\boldsymbol{\Omega},t-s/c)\Big\}\,\mathrm{d}s\,\mathrm{d}\Omega$$

for $m \le n \le N$, $0 \le m \le N$. Eq. (13) represents a set of simultaneous integral equations for the moments of intensity, and forms a complete description of the radiative transfer of interest, provided that Λ and I_w are specified. After the solutions of the moments of intensity are obtained from Eq. (13), any radiative physical quantity of interest, such as the source function or the intensity, can be easily found.

Physically, M_{11}, M^*_{11} and M_{10} are the u_1-, u_2- and u_3-components of radiative flux, respectively; that is,

$$\mathbf{q}(\mathbf{r},t) = M_{11}(\mathbf{r},t)\mathbf{e}_1(\mathbf{r}) + M^*_{11}(\mathbf{r},t)\mathbf{e}_2(\mathbf{r}) + M_{10}(\mathbf{r},t)\mathbf{e}_3(\mathbf{r}) \tag{14}$$

The domains of integration of the integrals on the right hand side of Eq. (13) may vary with time, and the moments of intensity at a given instant t depend on those before t. Thus, the integral equations are Volterra type. This feature is very different from the integral equations of time-independent radiative transfer, which are Fredholm type. However, in Eq. (13), if I_w is independent of time and let t approach infinity, the first term on the right hand side representing the contribution of the initial condition can be dropped, and only the second and the third terms standing for boundary irradiation and scattering contributions, respectively, are left. Then, the resulting expression is consistent with the formulation for time-independent radiative transfer in an absorbing and anisotropically scattering medium [21], provided that the angle integral (the second term) and the angle-distance integral (the third term) on the right-hand side of Eq. (13) are transformed into surface integral form and volume integral form, respectively.

If the medium considered is isotropically scattering, the set of integral equations reduces to one integral equation for M_{00}. The other high-order moments of intensity can be readily obtained by integration with the solved M_{00}. Besides, the integral equation of M_{00}, in essence, corresponds to the Peierls' equation in [18] for a gray, time-independent-property medium without internal source, provided that the integral representing scattering contribution is expressed in volume integral form.

3. Examples and numerical methods

With the integral equations for anisotropic scattering derived in Section 2, we are ready to apply the formulation to a problem often encountered in applications. The problem is the transient radiative transfer in a finite cylindrical medium (radius r_o and height z_o) exposed to a pulse radiation. The medium is assumed to be absorbing and linearly anisotropically scattering ($N = 1$). The spatial coordinate system is the conventional cylindrical coordinates, as shown in Fig. 1(b). The angle between the z axis and the direction of radiation propagation is θ whereas the directional azimuthal angle φ is measured from the rz plane, as shown in Fig. 1(b). We assume that the irradiation is a spatially uniform pulse normal to the circular bottom surface at $z = 0$, and the top and lateral surfaces are free from irradiation. The boundary irradiation $I_w(r, z, \mu, \varphi, t)$ can be expressed as

$$I_w(r,0,\mu,\varphi,t) = I_o F(t)\delta(\mu-1)\delta(\varphi), \quad \text{for } 0 \le r \le r_o,\ \mu > 0,\ 0 \le \varphi < 2\pi,\ t \ge 0 \tag{15a}$$

$$I_w(r,z_o,\mu,\varphi,t) = 0, \quad \text{for } 0 \le r \le r_o,\ \mu < 0,\ 0 \le \varphi < 2\pi,\ t \ge 0 \tag{15b}$$

$$I_w(r_o, z, \mu, \varphi, t) = 0,$$
$$\text{for } 0 \le z \le z_o,\ -1 \le \mu \le 1, \quad \pi/2 < \varphi < 3\pi/2,\ t \ge 0 \tag{15c}$$

where δ is the delta function, and the function F is defined as

$$F(t) = \exp\left[-4\ln 2\left(\frac{t - t_c}{t_p}\right)^2\right]. \tag{16}$$

The temporal shape of the pulse is a truncated Gaussian distribution. In Eq. (16), t_c is the time when the pulse reaches its maximum, and t_p presents the full width at half maximum (FWHM) for the temporal shape of $F(t)$. We assume that there is no radiation energy within the medium initially. Thus, the initial condition is

$$I(r, z, \mu, \varphi, 0) = 0, \quad \text{for } 0 \le r \le r_o,\ 0 \le z \le z_o,\ -1 \le \mu \le 1,\ 0 \le \varphi < 2\pi \tag{17}$$

With the initial and boundary conditions specified and considering the finite speed of radiation propagation, the integral equations of the moments of intensity for the axisymmetric medium can be expressed as

$$\begin{Bmatrix} M_{00}(r, z, t) \\ M_{10}(r, z, t) \\ M_{11}(r, z, t) \end{Bmatrix} = I_o F(t - z/c)\exp(-\beta z)\begin{Bmatrix} 1 \\ 1 \\ 0 \end{Bmatrix} H(ct - z) + \frac{1}{4\pi} H(ct - z)\int_0^{2\pi}\int_{-1}^{1}\int_0^{s_u(r,\,z,\,\mu,\,\varphi,\,t)} \beta\omega \times \exp(-\beta s)\begin{Bmatrix} 1 \\ \mu \\ \left[1 - \mu^2\right]^{1/2}\cos\varphi \end{Bmatrix} \times \left\langle M_{00}\left[r'(r, s, \mu, \varphi), z'(z, s, \mu), t - s/c\right] + a_1\left\{\mu M_{10}\left[r'(r, s, \mu, \varphi), z'(z, s, \mu), t - s/c\right] + \frac{\left[r\left(1 - \mu^2\right)^{1/2}\cos\varphi - s\left(1 - \mu^2\right)\right]}{r'(r, s, \mu, \varphi)} \times M_{11}\left[r'(r, s, \mu, \varphi), z'(z, s, \mu), t - s/c\right]\right\}\right\rangle \mathrm{d}s\,\mathrm{d}\mu\,\mathrm{d}\varphi \tag{18}$$

and M_{11}^* (the ψ-component of radiative flux) is zero, since the irradiation on the constant property medium is axisymmetric. In Eq. (18), we define

$$r'(r, s, \mu, \varphi) = \left[r^2 - 2rs\left(1 - \mu^2\right)^{1/2}\cos\varphi + s^2\left(1 - \mu^2\right)\right]^{1/2} \tag{19}$$

$$z'(z, s, \mu) = z - s\mu \tag{20}$$

$$s_u(r, z, \mu, \varphi, t) = \min\left\{(ct - z)/(1 - \mu), s_w(r, z, \mu, \varphi)\right\} \tag{21}$$

where $\min\{x, y\}$ denotes the smaller value of x and y, and s_w is the distance from the considered point labeled by r and z to the nearest point on the medium boundary seen from the considered point reversely along the direction denoted by μ and φ. It is readily found that

$$s_w(r, z, \mu, \varphi) = \begin{cases} -(z_o - z)/\mu, & \text{if } -1 \le \mu < \mu_1(r, z, \varphi) \\ \zeta(r, \varphi)/\left(1 - \mu^2\right)^{1/2}, & \text{if } \mu_1(r, z, \varphi) \le \mu \le \mu_2(r, z, \varphi) \\ z/\mu, & \text{if } \mu_2(r, z, \varphi) < \mu \le 1 \end{cases} \tag{22}$$

with

$$\mu_1(r, z, \varphi) = -\cos\left\{\arctan\left[\frac{\zeta(r, \varphi)}{(z_o - z)}\right]\right\} \tag{23}$$

$$\mu_2(r, z, \varphi) = \cos\left\{\arctan\left[\frac{\zeta(r, \varphi)}{z}\right]\right\} \tag{24}$$

$$\zeta(r, \varphi) = r\cos\varphi + \left(r_o^2 - r^2\sin^2\varphi\right)^{1/2} \tag{25}$$

In Eq. (18), the upper limit of integration over s, s_u, is a function of r, z, μ, φ and t. As shown in Eq. (18), s_u represents the length determining the domain of dependence of the moments of intensity at the position denoted by r and z. The domain of dependence may vary with time and the radiative transfer is confined in the domain due to either the finite propagation time or the finite volume of the medium. The derivation of s_u is similar to that stated in [16], and so it is not duplicated here.

When the medium is unbounded in the r-direction (r_o approaches infinity) and the irradiation pulse is uniform, Eq. (18) reduces to the equations for a planar medium. The resulting equations can be expressed as

$$\begin{Bmatrix} M_{00}(z,t) \\ M_{10}(z,t) \end{Bmatrix} = I_o F(t-z/c)\exp(-\beta z)H(ct-z) + \frac{1}{2}H(ct-z)\int_{-1}^{1}\int_{0}^{s_u(z,\mu,t)} \beta\omega \times \exp(-\beta s)\begin{Bmatrix} 1 \\ \mu \end{Bmatrix} \times \left\{M_{00}(z-s\mu, t-s/c) + a_1\mu M_{10}(z-s\mu, t-s/c)\right\} ds\, d\mu$$

where

$$s_u(z,\mu,t) = \begin{cases} \min\{(ct-z)/(1-\mu), -(z_o-z)/\mu\}, & \text{if } -1 \le \mu < 0 \\ (ct-z)/(1-\mu), & \text{if } \mu = 0 \\ \min\{(ct-z)/(1-\mu), z/\mu\}, & \text{if } 0 < \mu \le 1 \end{cases}$$

In the 1D problem, the moments of intensity are independent of r, and the r-component of radiative flux, M_{11}, is zero as well as M_{11}^*. Thus, only the two integral equations of M_{00} and M_{10} are required to be solved.

The method adopted to solve the integral equations of the moments of intensity for the 1D and 2D anisotropic scattering problems is the QM [16], which uses a product quadrature rule to approximate the angle-distance integral in Eqs. (18) and (26). This method transforms the integral equations to a system of algebraic equations and has been successfully used to solve 1D transient radiative transfer in a planar isotropically scattering medium. The details of the QM for the 1D problem can be found in [16], and so only the adaptation for the 2D problem is briefly described here.

From Eqs. (21) and (22), it is readily found that s_u has a non-continuous first-order derivative with respect to μ. In the interest of accuracy, we split the integration interval of μ into subintervals, over which the first-order derivative of s_u is continuous. Besides, for accuracy of the evaluation of half-range radiative fluxes on the boundaries, the integration interval of φ is split into four subintervals, $[0, \pi/2]$, $[\pi/2, \pi]$, $[\pi, 3\pi/2]$, and $[3\pi/2, 2\pi]$. Then, we adopt the product Gaussian-Legendre quadrature to evaluate each subintegral. In each integral, N_φ-, N_μ- and N_s-point quadrature rules are used for the φ, μ and s integrations, respectively.

The distributions of the moments of intensity are approximated by their values at given grid points associated with interpolation. For simplicity, we use a uniform grid in the r-, z- and t-directions, where Δr, Δz and $\Delta t = \Delta z/c$ are the grid sizes in the r-, z- and t-directions, respectively. However, the quadrature points used to evaluate the angle-distance integrals are very often not located exactly on the uniform grid points. The scattering parts of the moments of intensity at the quadrature points are obtained by interpolation in terms of those at the grid points neighboring in space and time. The interpolation procedure for the 2D problem is very similar to that in [16]. Since the moments of intensity depend on r, z and t for the 2D problem, interpolation in three-dimension is required. After the interpolation procedure in the z- and t-directions is performed, an additional interpolation in the r-direction needs to be done. While bi-quadratic interpolation is adopted for the 1D problem as in [16], trilinear interpolation is used here for the 2D problem to simplify programming. The above procedure transforms the integral equations into a system of algebraic equations. Solving the system iteratively at each time step, we can obtain the moments of intensity at the grid points as stated in [16].

To validate the results obtained by the QM, we also solve the problems by the Monte Carlo methods. For the 1D problem, we adopt the conventional Monte Carlo method (CMCM) [8]. The reverse (or backward) Monte Carlo method [22,23] (RMCM) provides better results of the moments of intensity at a specified point than the CMCM does. Thus, we adapt the RMCM developed for steady problems to solve the transient 2D problem.

4. Results and discussions

4.1. One-dimensional problem

Transient radiative transfer in a planar isotropically scattering medium exposed to a collimated pulse radiation has been studied in [16]. The influence of the scattering albedo and the optical thickness on the transient radiative transfer has been investigated. Hence, in this work, we aim at the effects of the anisotropic scattering. We consider two values of a_1, 1.0 and -1.0, for planar conservative ($\omega = 1.0$) media with the pulse of $c\beta t_c = 1.0$ and $c\beta t_p = 0.333$. The distributions of the reflectivities $M_{10}^-(0, t)/I_o = [I_o F(t)H(t) - M_{10}(0, t)]/I_o$ and of the transmissivities $M_{10}(z,t)/I_o$ for $\beta z_o = 5.0$ and 0.2 over dimensionless time ($c\beta t$) are shown in Figs. 2 and 3, respectively. The QM results are generated by using $N_\mu = 12$, $N_s = 16$ and $z_o/\Delta z = 80$ for $\beta z_o = 5.0$, and $N_\mu = 24$, $N_s = 12$ and $z_o/\Delta z = 30$ for $\beta z_o = 0.2$. The combinations of the quadrature points and the grid sizes have been shown to generate accurate results [16]. The results solved by the CMCM are also shown in the figures to validate the present QM results. In the computation of the CMCM, a very large number of bundles, 10^8, are used for each of the cases to reduce the statistical errors inherent within the CMCM results and to ensure the accuracy. From Figs.

2 and 3, it is found that the results by the QM and CMCM agree very well for the duration shown.

In Fig. 2, the reflectivity for $a_1 = 1.0$ (forward-scattering dominating) has a smaller value than that for $a_1 = -1.0$ (backward-scattering dominating) around the peaks of the reflectivity curves. This is because, the radiation scattered once is the dominant contributor of the reflectivity and the strongly backward scattering makes more radiation be scattered back. Moreover, when the irradiation pulse penetrates deep into the medium, the reflectivity for $a_1 = 1.0$ becomes larger than that for $a_1 = -1.0$ for the optically thick case. More radiation energy for the forward-scattering dominating case can reach the center of the medium than that for the backward-scattering dominating case can. After the irradiation pulse passes through the medium, the scattered radiation energy mainly transfers from the center of the medium to the boundary surfaces, and then leaves the medium. The forward scattering tends to enhance such radiative transfer, and makes more radiation energy be carried to the boundary. Therefore, more radiation energy leaves the medium and results in the larger reflectivity of the forward-scattering dominating case. On the other hand, around the peak instant, the transmissivity for $a_1 = 1.0$ keeps larger than that for $a_1 = -1.0$. This is because, the forward scattering makes more radiation energy penetrate through the medium in the direction of the irradiation, and enhances the radiative transfer from the center to the boundary at later instants. Next, it is found that far away from the reflectivity and the transmissivity peak instants, both the reflectivity and the transmissivity for $a_1 = 1.0$ become smaller than those for $a_1 = -1.0$ for this optically thick case ($\beta z_o = 5.0$). Because more energy has escaped from the medium for the forward-scattering case, less energy is eventually left within the medium and the reflectivity and the transmissivity for the case are smaller. Besides, the reflectivity curves eventually merge with the transmissivity curves for each of the anisotropically scattering cases as $c\beta t$ becomes large enough.

In Fig. 3, similar tendency can also be observed from the results of the optically thin case ($\beta z_o = 0.2$). However, unlike the optically thick case, the values of the reflectivity for $a_1 = -1.0$ for the optically thin case always keep larger than those for $a_1 = 1.0$ for the duration shown. This is because, not only the penetration of radiation through a small optical thickness is very easy, but also the forward scattering enhances the penetration. Thus, after the irradiation pulse passes, the radiation energy left within the medium decreases so quickly that the reflectivity for $a_1 = 1.0$ has no chance to become larger than that for $a_1 = -1.0$. Similar to the result shown in Fig. 2, Fig. 3 reveals that more radiative energy remains within the medium for the backward-scattering dominating case than that for the forward-scattering dominating case does for large $c\beta t$.

4.2. Two-dimensional problem

Here, the QM is adopted to predict the transient radiative transfer within 2D finite cylindrical scattering media; isotropic as well as anisotropic scattering is considered. The irradiation pulse is characterized by $c\beta t_c = 1.0$ and $c\beta t_p = 0.333$. The convergence of the QM is examined first. Conceptually, the finer meshes

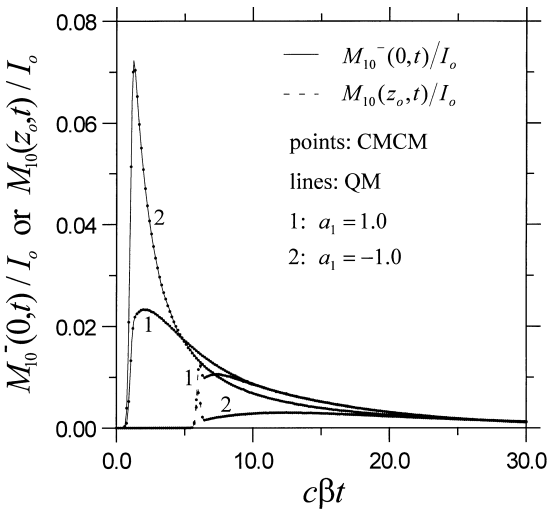

Fig. 2. The results of the reflectivities and the transmissivities obtained by the QM and CMCM for 1D planar linearly anisotropically scattering media of $\beta z_o = 5.0$.

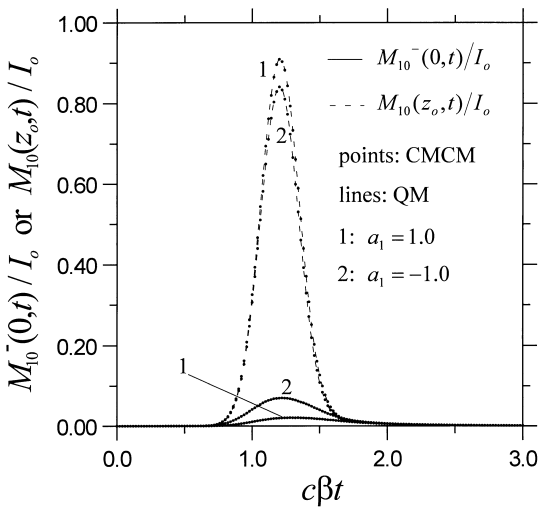

Fig. 3. The results of the reflectivities and the transmissivities obtained by the QM and CMCM for 1D planar linearly anisotropically scattering media of $\beta z_o = 0.2$.

and the higher order quadrature rules yield the more accurate results. To check the influence of the number of the grid points, in Fig. 4 we plot the QM results generated by using 11×11, 21×21, 31×31 and 41×41 grid points with $N_\varphi = N_\mu = 10$ and $N_s = 40$, respectively, for a conservative medium of $\beta r_o = \beta z_o = 1.0$. We choose the half-range radiative flux $M_{10}^-(0, 0, t) = I_o F(t)H(t) - M_{10}(0, 0, t)$ as the exemplified results since it is the result of scattered radiation. From Fig. 4, it is found that the results obtained by using the fewer grid points almost coincide with the 41×41 grid point results, except around the peak of $M_{10}^-(0,0,t)$. Thus, for the moderate optical size medium we find that the 21×21 mesh can provide converged results. However, with a further examination, we find that the larger optical size is, the more grid points are required to provide converged results. In addition, to investigate the dependence of the QM results on the quadrature points, the $M_{10}^-(0, 0, t)$ results obtained by using various order quadrature rules are plotted in Fig. 5. Here, we consider four sets of $N_\varphi = N_\mu$ and N_s. As shown in Fig. 5, only the results of $N_\varphi = N_\mu = 3$ and $N_s = 12$ have obvious small deviations apart from those of $N_\varphi = N_\mu = 10$ and $N_s = 40$, and the other result curves almost coincide. Thus, the product quadrature rule of $N_\varphi = N_\mu = 7$ and $N_s = 30$ is employed here for the latter cases.

Fig. 6 shows the effects of ω on the transient radiative transfer within the isotropically scattering ($a_1 = 0.0$) medium; the results of $M_{10}^-(0 ,0, t)$ and $M_{10}(0, z_o, t)$ are shown. We also plot the results obtained by the RMCM in Fig. 6, to validate the QM results. Here, each RMCM result is generated by using 500,000 bundles to keep the inherent random errors far smaller than the absolute values of the RMCM solutions. As shown in Fig. 6, the results obtained by the QM and RMCM are in excellent agreement for a wide range of ω. Both $M_{10}^-(0, 0, t)$ and $M_{10}(0, z_o, t)$ increase with the increase of ω at any time, and both of them for a larger ω have longer tails. For each case shown, the $M_{10}^-(0, 0, t)$ curve finally merges with the corresponding $M_{10}(0, z_o, t)$ curve as $c\beta t$ increases. This phenomenon is very similar to that observed in the 1D problem, and it reveals that the distribution of scattered radiative energy finally becomes symmetrical about the $z = z_o/2$ plane. After we carefully examine the distribution of M_{00}, the symmetrical distribution is confirmed.

In Fig. 7, we plot the QM results of $M_{10}^-(0, 0, t)$ for three optical sizes. The media are conservative and of identical optical radius $\beta r_o = 1.0$, but of different optical heights, $\beta z_o = 2.0$, 1.0, and 0.5, respectively. For comparison purpose, the reflectivity curve for a 1D planar medium of $\beta z_o = 0.5$ is also shown in Fig. 7. The $M_{10}^-(0, 0, t)$ curves for the three 2D cases coincide for small $c\beta t$, and the curves for the smaller βz_o cases are successively apart from those for the larger βz_o cases, as shown in Fig. 7. A similar trend for a 1D planar medium has been found and explained [16]. For a 1D planar medium, except the peak, only a single kink results from the finite thickness of the medium, as shown by the 1D reflectivity curve. However, except the peak, two kinks are often observed for the 2D problem, as exhibited by the curves of the $\beta z_o = 1.0$ and 2.0 cases, although the second kink for the $\beta z_o = 2.0$ case is not obvious. The finite radius of the medium is responsible for the first of them, while the finite height causes the other. The occurrence instants for

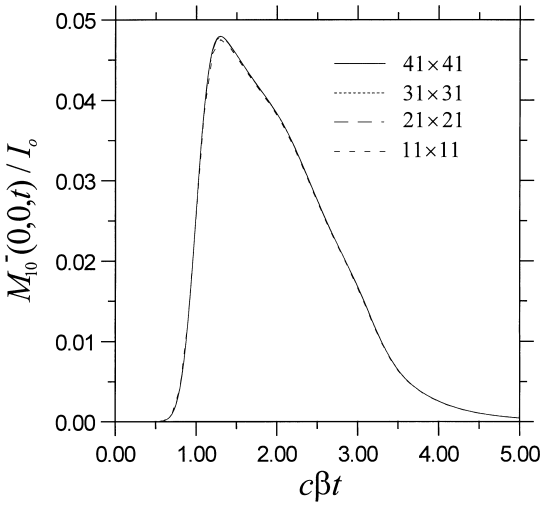

Fig. 4. The dependence of the 2D QM results of $M_{10}^-(0, 0, t)$ on the number of the grid points.

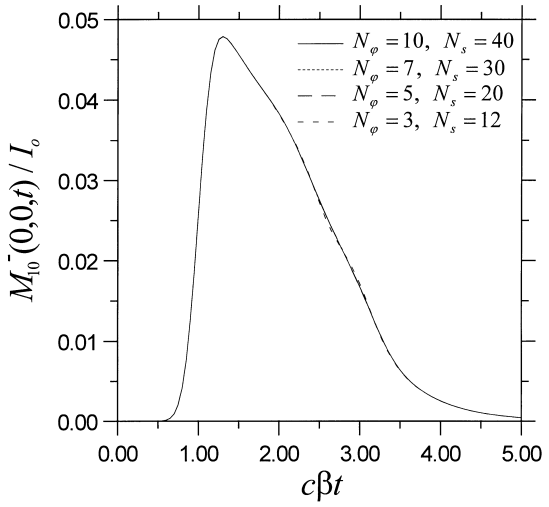

Fig. 5. The dependence of the 2D QM results of $M_{10}^-(0, 0, t)$ on the number of the quadrature points.

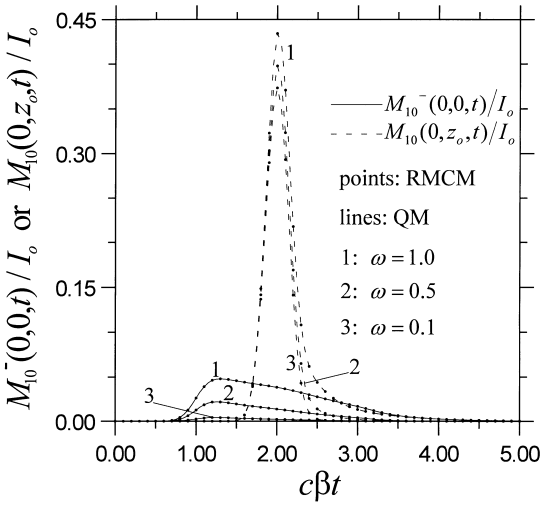

Fig. 6. The results of $M_{10}^{-}(0, 0, t)$ and $M_{10}(0, z_o, t)$ obtained by the QM and RMCM for 2D finite cylindrical media with various values of ω.

the two kinks are around $c\beta t_c + 2\beta z_o$ and $c\beta t_c + \beta r_o$, respectively, provided that the width of pulse t_p is far smaller than z_o/c and r_o/c. In Fig. 7, the curve of the $\beta z_o = 0.5$ case, seems to have only one kink like that of the 1D planar medium. This is because the "two" kinks happen nearly about the same time due to the particular aspect ratio $z_o/r_o = 0.5$ for the $\beta z_o = 0.5$ case.

Next, we consider the effects of a_1 on $M_{10}^{-}(0, 0, t)$ and $M_{10}(0, z_o, t)$ for a 2D conservative medium of $\beta r_o = \beta z_o = 1.0$. The $M_{10}^{-}(0, 0, t)$ and $M_{10}(0, z_o, t)$ obtained by the QM for $a_1 = 1.0$ and $a_1 = -1.0$ are shown in Fig. 8. In addition, the isotropic scattering results are also plotted in Fig. 8 for comparison. As shown in Fig. 8, the flux primarily due to the penetrating pulse, that is, the $M_{10}(0, z_o, t)$ for small $c\beta t$, for the forward-scattering dominating case is larger than that for the backward-scattering dominating case. On the other hand, the fluxes due to scattered radiation, that is, the $M_{10}^{-}(0, 0, t)$ for all $c\beta t$ and the $M_{10}(0, z_o, t)$ for large $c\beta t$, have larger values for the backward-scattering dominating case. Besides, the $M_{10}^{-}(0, 0, t)$ and the $M_{10}(0, z_o, t)$ curves for either of the anisotropic scattering cases eventually merge individually as $c\beta t$ increases, as shown in the isotropic scattering case. Thus, as the time passes, the distributions of the scattered radiative energy gradually become symmetrical about the central plane $z = z_o/2$, no matter whether the scattering is isotropic or anisotropic.

In Fig. 9, we plot the spatial distributions of $M_{10}^{-}(r, 0, t) = I_o F(t) H(t) - M_{10}(r, 0, t)$, $M_{10}(r, z_o, t)$ and $M_{11}(r_o, z, t)$ at some instants of interest, respectively. Both the QM and RMCM results are shown in Fig. 9. The results by the two methods are in good agreement, and only very small discrepancies are found in the $M_{10}^{-}(r, 0, t)$ curves for the early instants and around the peaks of the $M_{11}(r_o, z, t)$ curves. The discrepancies are primarily due to the RMCM random errors. Besides, the non-smooth variations of the $M_{10}^{-}(r, 0, t)$ curves near the lateral boundary and of the $M_{11}(r_o, z, t)$ curves around the peaks are caused by the finite grid points of the QM. They can be readily smoothed by using a finer mesh.

In Fig. 9(a), the distributions of $M_{10}^{-}(r, 0, t)$ around the center at the early time before the peak instant, $c\beta t = 1.0$, are more uniform than those at an instant

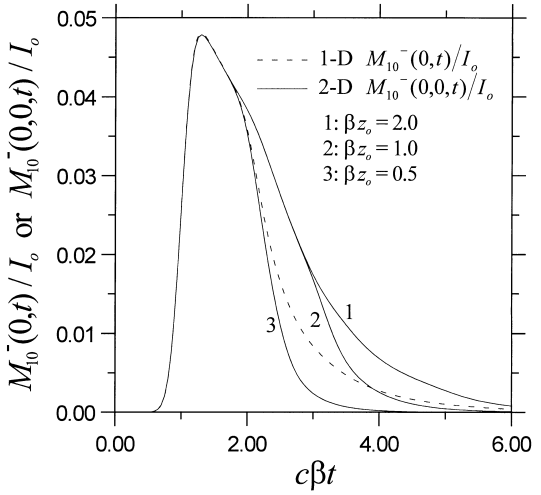

Fig. 7. The QM results of $M_{10}^{-}(0, 0, t)$ for 2D finite cylindrical conservative media of three optical sizes.

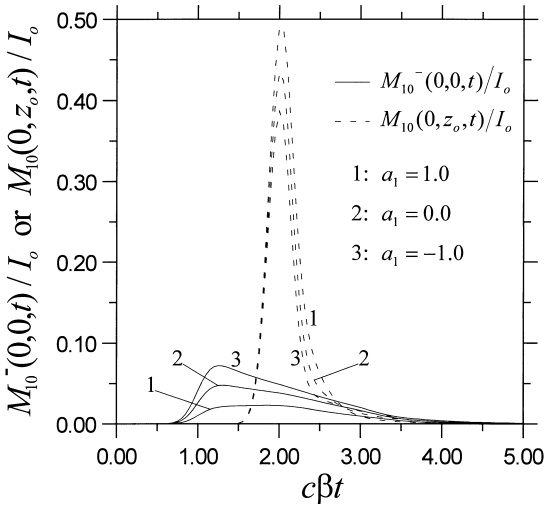

Fig. 8. The results of $M_{10}^{-}(0, 0, t)$ and $M_{10}(0, z_o, t)$ obtained by the QM and RMCM for 2D finite cylindrical conservative media with various values of a_1.

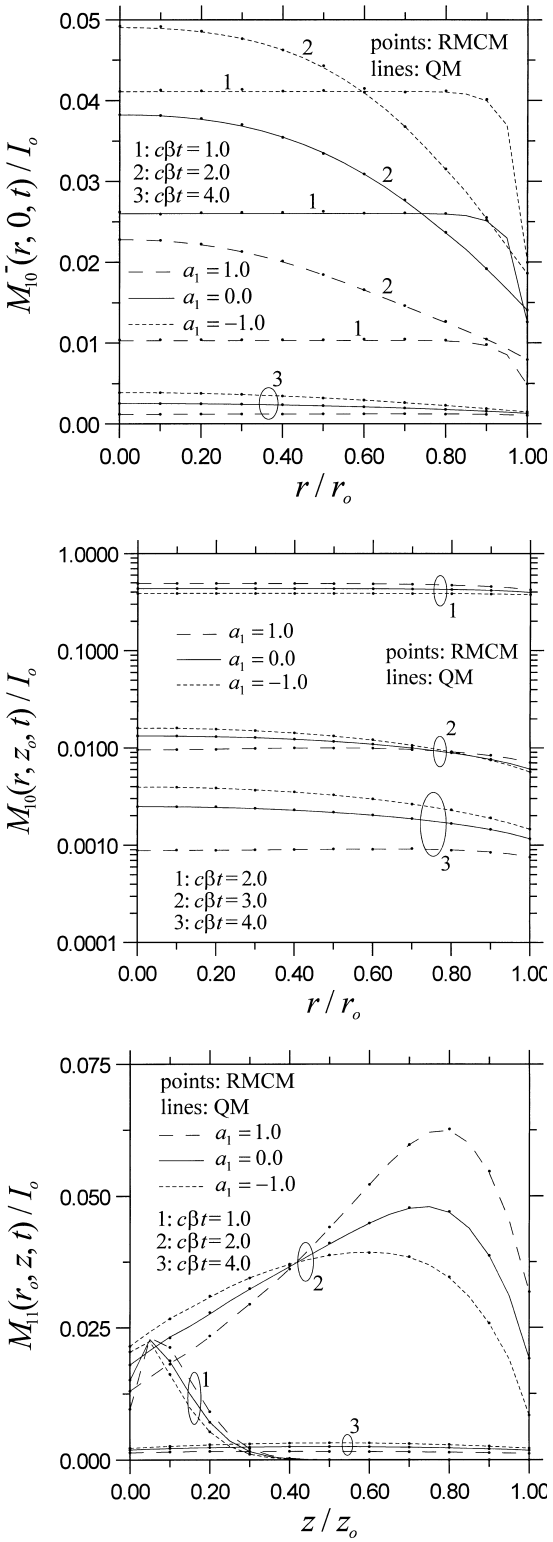

Fig. 9. The results at some instants of interest obtained by the QM and RMCM for 2D finite cylindrical conservative media with various values of a_1; (a) the spatial distributions of $M_{10}^{-}(r, 0, t)$; (b) the spatial distributions of $M_{10}(r, z_o, t)$; (c) the spatial distributions of $M_{11}(r_o, z, t)$.

after the peak instant, say $c\beta t = 2.0$. This is caused by the smaller radiation penetrating distance in the z-direction at the earlier time. With a smaller penetrating distance, the effective aspect ratio of the medium becomes smaller and the values of $M_{10}^{-}(r, 0, t)$ around the center become closer to those of a 1D planar medium. Besides, comparing the distributions of $M_{10}^{-}(r, 0, t)$ at $c\beta t = 1.0$ and those of $M_{10}(r, z_o, t)$ at $c\beta t = 2.0$, we can find that the spatial distributions of the $M_{10}^{-}(r, 0, t)$ have larger changes near the lateral boundary. The major contributor of the $M_{10}(r, z_o, t)$ is the attenuated collimated radiation, which directly penetrates the medium without scattering, and the attenuated collimated radiation is uniformly distributed on any surface z = constant. On the other hand, the $M_{10}^{-}(r, 0, t)$ completely results from scattered radiation. Thus, the spatial distributions of the $M_{10}(r, z_o, t)$ are more uniform than those of the $M_{10}^{-}(r, 0, t)$.

Fig. 9(c) shows that the locations of the peaks of the radiative flux through the lateral boundary vary with the time. For the isotropically and anisotropically scattering cases, at the early instant $c\beta t = 1.0$, the peaks appear near the bottom surface $z = 0$, then the peaks shift following the peak of the pulse irradiation along the positive z-direction. At the late instant $c\beta t = 4.0$, the maxima appear at the central location $z = z_o/2$, and the spatial distributions of the $M_{11}(r_o, z, t)$ become almost symmetrical about the maxima. This is a direct result of the symmetrical distribution of the scattered radiation energy remaining within the medium at large time. From Figs. 8 and 9, we can find that the temporal distribution of the transient radiative transfer strongly depends on the anisotropic scattering.

The CPU time required by the QM to solve one of the isotropic scattering cases by using 21×21 spatial grid points, 100 time steps, $N_\varphi = N_\mu = 10$ and $N_s = 40$ is about 5100 s on a DEC Alpha 8400 computer. This CPU time is about 1/550 of that required by the RMCM to generate the same number of results by employing 500,000 bundles. For an anisotropically scattering case, the ratio of the required CPU times becomes smaller.

5. Concluding remarks

The integral equation formulation for transient radiative transfer in a 3D anisotropically scattering medium is presented. The exemplified 1D and 2D anisotropically scattering problems are solved by the QM

and Monte Carlo methods. With the comparisons of the results for a variety of cases, it is found that the solutions based on the exact integral equation formulation are effective, and of high accuracy. The results show that the effects of anisotropic scattering are strong for the transient problems considered.

References

[1] N.J. McCormick, Remote characterization of a thick slab target with a pulsed laser, J. Opt. Soc. Am. 72 (1982) 756–759.

[2] R.A. Elliott, Multiple scattering of optical pulses in scale model clouds, Applied Optics 22 (1983) 2670–2681.

[3] K. Mitra, S. Kumar, Application of transient radiative transfer equation to oceanographic lidar, in: Proceedings of the 1997 ASME International Mechanical Engineering Congress and Exposition, vol. 3, ASME, Fairfield, 1997, pp. 359–365.

[4] Y. Yamada, Light-tissue interaction and optical imaging in biomedicine, in: C.L. Tien (Ed.), Annual Review of Heat Transfer, vol. 6, Begell House, New York, 1995 Chap. 1.

[5] B.C. Wilson, M.S. Patterson, The physics of photodynamic therapy, Phys. Med. Biol. 31 (1986) 327–360.

[6] M.Q. Brewster, Y. Yamada, Optical properties of thick, turbid media from picosecond time-resolved light scattering measurements, Int. J. Heat Mass Transfer 38 (1995) 2569–2581.

[7] K.K. Hunt, N.J. McCormick, Numerical test of an inverse method for estimating single-scattering parameters from pulsed multiple-scattering experiments, J. Opt. Soc. Am. A 2 (1985) 1965–1971.

[8] B.C. Wilson, G. Adam, A Monte Carlo model for the absorption and flux distributions of light in tissue, Med. Phys. 10 (1983) 824–830.

[9] C.I. Rackmil, R.O. Buckius, Numerical solution technique for the transient equation of transfer, Numerical Heat Transfer 6 (1983) 135–153.

[10] S. Ito, K. Furutsu, Theory of light pulse propagation through thick clouds, J. Opt. Soc. Am. 70 (1980) 366–374.

[11] K. Mitra, S. Kumar, Development and comparison of models for light-pulse transport through scattering–absorbing media, Applied Optics 38 (1999) 188–196.

[12] Y. Yamada, Y. Hasegawa, Time-dependent FEM analysis of photon migration in biological tissues, JSME Int. J. B 39 (1996) 754–761.

[13] K. Mitra, M.-S. Lai, S. Kumar, Transient radiation transport in participating media within a rectangular enclosure, J. Thermo. Heat Transfer 11 (1997) 409–414.

[14] A.L. Crosbie, R.G. Schrenker, Multiple scattering in a two-dimensional rectangular medium exposed to collimated radiation, J. Quant. Spectrosc. Radiat. Transfer 33 (1985) 101–125.

[15] J.-M. Zhang, W.H. Sutton, Predictions of radiative transfer in two-dimensional nonhomogeneous participating cylindrical media, J. Thermo. Heat Transfer 10 (1996) 47–53.

[16] C.-Y. Wu, Propagation of scattered radiation in a participating planar medium with pulse irradiation, J. Quant. Spectrosc. Radiat. Transfer (1999) (accepted).

[17] D.I. Nagirner, Theory of nonstationary transfer of radiation, Astrofizika 10 (1974) 445–469.

[18] G.C. Pomraning, The Equations of Radiation Hydrodynamics, Pergamon, Oxford, 1973 (Chapter 2).

[19] C.M. Chu, S.W. Churchill, Representation of the angular distribution of radiation scattered by a spherical particle, J. Opt. Soc. Am. 45 (1955) 958–962.

[20] G.E. Hunt, The transport equation of radiative transfer in a three-dimensional space with anisotropic scattering, J. Inst. Maths. Applics 3 (1967) 181–192.

[21] C.-Y. Wu, Exact integral formulation for radiative transfer in an inhomogeneous scattering medium, J. Thermo. Heat Transfer 4 (1990) 425–431.

[22] D.V. Walters, R.O. Buckius, Monte Carlo methods for radiative heat transfer in scattering media, in: C.L. Tien (Ed.), Annual Review of Heat Transfer, vol. 5, CRC, Boca Raton, 1994 (Chapter 3).

[23] D.M. O'Brien, Accelerated Quasi Monte Carlo integration of the radiative transfer equation, J. Quant. Spectrosc. Radiat. Transfer 48 (1992) 41–59.